


Centralized dynamic frequency allocation for cell-edge demand satisfaction in fractional frequency reuse networks

Maryum Hina¹ · Sarmad Sohaib¹ 

Published online: 20 January 2017
© Springer Science+Business Media New York 2017

Abstract Fractional frequency reuse (FFR) has emerged as a well-suited remedy for inter-cell interference reduction in the next-generation networks by allocating frequency reuse factor (FRF) of unity for the cell-center (CC) and higher FRF for the cell-edge (CE) users. However, this strict FFR comes at a cost of equal partitioning of frequency resources to the CE which most likely has varying demands in current networks. In order to mitigate this, we propose a centralized dynamic resource allocation scheme which allocates demand-dependent resources to CE users. The proposed scheme therefore outperforms the fixed allocation scheme of strict FFR for both CC and CE users. Complexity analysis provides a fair means of analyzing the suitability of proposed algorithm. We have also compared the proposed methodology with a reference dynamic fractional frequency reuse (DFFR) scheme. Results show maximum performance gain of up to 30% for 3 reference cells employing Rayleigh fading—through normalized area spectral efficiency (ASE) analysis for both fixed allocation and DFFR. Spectral efficiency analysis also indicates per-cell performance gain for both CC and CE users. Further, detailed three-dimensional ASE plots give insights into the affects to other cells. Due to dynamic nature of traffic loads, the proposed scheme is a candidate solution for satisfying the demands of individual cells.

Keywords Fractional frequency reuse · Strict FFR · Dynamic resource partitioning · Cell-edge · Area spectral efficiency · Spectral efficiency

✉ Sarmad Sohaib
sarmad.sohaib@uettaxila.edu.pk

¹ University of Engineering and Technology, Taxila, Pakistan

1 Introduction

The diversified usage of cellular phones in the context of data services has led to an immense increase in data-rate demands in the next generation cellular networks e.g. LTE and WiMAX. To cope with these high data-rate demands, orthogonal frequency division multiple access (OFDMA) has emerged as an attractive solution as it employs orthogonal sub-carriers thereby nullifying the loss due to the inter-symbol interference. To further enhance the network capacity, excessive reuse of frequency sub-carriers is highly demanded. Various resource reuse schemes have been proposed in the literature, for instance a comprehensive survey is available in [1]. The suggested full frequency reuse or unity-reuse scheme allocates the whole bandwidth to each cell giving rise to an increased spectral efficiency (SE) but at the cost of increased inter-cell interference (ICI). A reuse- Δ scheme splits the whole band into Δ sub-bands and allocates orthogonal sub-carriers to each cell, thereby reducing ICI but at the cost of reduced SE. A good compromise between SE and ICI mitigation is fractional frequency reuse (FFR) also referred to as strict FFR or hard FFR in the literature. It employs frequency reuse factor (FRF) of unity for close-to-base station users also called cell-center (CC) users, and a higher FRF for cell-edge (CE) users [2]. A variant of strict FFR is soft FFR (SFR) which allows full frequency reuse in each cell with certain power bound for the CE regions [3]. Much of the research in literature has compared the versions of FFR schemes [3–6]. Strict FFR has been reported as more energy efficient than SFR for fully loaded cells and at high signal to interference plus noise ratio (SINR) regime [4]. It suits well in terms of sum-rate, coverage probability, and for CE users as compared to the SFR [3,6]. With this motivation, we have considered strict FFR as the reference scheme in this paper.

Static reuse schemes partition the resources among the CC and the CE users depending upon the geographical area covered by these regions, therefore making the allocation well-determined and preplanned [5,7–9]. In [5], FFR and SFR were analytically evaluated for area spectral efficiency (ASE) performance on the metrics of normalized distance threshold, cell loading, and generalized FRF. Two scheduling schemes, round robin and max-SINR were presented in [7] for exploiting the tradeoff between the distance threshold and the number of users. The impact of reuse factor and distance threshold on selection of optimal FFR scheme in highly dense networks are analyzed in [10,11]. FFR scheme allocating bandwidth to the CC and the CE areas being partitioned into discrete regions with identically distributed ICI is proposed in [8,12]. Various tradeoffs between the distance threshold and bandwidth partitioning between the CC and the CE areas were observed for the two extreme scheduling schemes; round robin and greedy scheduling. Strict FFR and SFR were analyzed in [9] in the context of coverage probability and sum-rate employing point Poisson process (PPP) for the base station (BS) locations.

1.1 Related work

Dynamic allocation in FFR [13–21] is currently an active research area due to the CE region users being more exposed to ICI, and the vastly changing demands of the next generation users. In dynamic FFR the resources such as time [14], power [22,23], frequency [15] and a combination [13] are adjusted according to the dynamics of traffic load and/or channel conditions. In [15] the dynamic frequency allocation algorithm satisfies the minimum data-rate demands but the CE user performance is shown to be significantly reduced. Efficient and dynamic resource allocation algorithm for CE enhancement in non-orthogonal multiple access (NOMA) is discussed in [13]. Reuse factor selection via convex optimization [16] and optimal bandwidth selection via simulations depending upon user satisfaction is proposed in [17]. A grade of service (GoS) fair method for real-time traffic was proposed in [18] where the bandwidth of CC and CE regions was partitioned on the basis of number of users in each region given their SINR demands were satisfied. More recently, a distributed dynamic approach for frequency allocation (DDFFA) is proposed for the relay-based cellular networks (RBCNs) [19] employing coloring based distributed frequency allocation (C-DFA) and inter-BS as well as inter relay station (inter-RS) cooperation [24,25]. The dynamic scheme in [20,26] incorporates the self-organizing network (SoN) functionality for the FFR resource partition thereby enhancing the network throughput and call drop rate under varying network traffic. Another distributed dynamic FFR scheme is proposed in [27] employing cellular automata and center of gravity for sector-based resource allocation. To overcome the

performance degradation at the CE users, various techniques have been proposed in literature [21,28–31]. The centralized and distributed dynamic resource allocation via inter-cell interference coordination (ICIC) have been proposed in [28] and [32] respectively for CE performance enhancement. These schemes restrict some of the resources to be utilized when potential interference is experienced but are computationally complex. Employing cooperative MIMO (CoMP) at the CE is another way to alleviate CE user performance [29,30]. A dynamic approach for the FFR-based scheme is proposed in [31] where the stochastic geometry aids the capacity density and the area based frequency allocation for the CE-sector is made. However, their analysis was supported by simulations only and for a PPP BS deployment which gives rise to Voronoi tessellation of cells. Another sector-based dynamic strict FFR (DSFFR) scheme is proposed in [33]. DSFFR is proposed for small-cell based (heterogeneous) networks and joint scheduling performs resource allocation to different sectors of small-cell. A new dynamic fractional frequency reuse (DFFR) scheme is proposed in [21]. DFFR allocates CE resources similar to strict FFR except that a certain percentage of CE resources are shared among the cluster cells. These shared CE resources are allocated to the cell with increased CE traffic and thus dynamics of traffic demands are taken care of.

1.2 Paper contributions

One of the major drawbacks of the existing static FFR schemes is that they greatly ignore the impact of enhanced and possibly rapidly varying data-demands of the CE users that are inherent in the next-generation wireless networks [21]. Owing to the aforementioned fact, equally partitioning the sub-bands among the edge regions of a cluster of cells can severely degrade the rate performance of some of the cells. To the best of authors' knowledge, the effect of dynamic partitioning of resources among CE regions with varying demands has not been addressed especially when the BSs are pre-planned and well-defined as in a grid model.

In this paper, we present ASE analysis to analyze the impact of area-based dynamic resource partitioning. SE analysis indicates the per-cell performance gain for both CC and CE users. The three dimensional (3D) plots are presented to better visualize some existing tradeoffs between the frequency resources and the distance threshold. Finally, the effect of proposed dynamic partitioning on the *other* cells' performance is also presented. We have compared our work with a state-of-the-art DFFR scheme proposed in [21]. Analysis is provided for per-cell CC and CE spectral efficiencies as well as normalized average SEs for CC and CE users.

The remainder of this paper is organized as follows. Section 2 presents the considered downlink system model with an introduction to the static FFR scheme and received

SINR. Section 3 discusses the proposed sub-carrier allocation algorithm for which ASE analysis is presented in Sect. 4. Analytical results showing the considerable performance enhancement are presented in Sect. 5, and the work concludes in Sect. 6. For the sake of convenience throughout this paper, $\mathbb{E}[\cdot]$ presents the statistical expectation operator, $\mathcal{M}(\cdot)$ presents the moment generating function (MGF), and the coordinates (r, θ) are the location of a user and/or a BS in the polar coordinate system.

2 Downlink system model

In this work, a downlink OFDMA multi-cell network employing FFR is considered. In the considered grid model, BSs are equipped with omni-directional antennas and are assumed to be located at the center of the hexagonal cell. Uniform distribution is considered for randomly located mobile users making the resource partitioning between CC and CE users conveniently on the basis of geographical cell partitioning of the respected areas. Every cell with a radius R is partitioned into CC area having radius R_c which gives rise to the normalized inner radius $r_n = \frac{R_c}{R}$, where $r_n \in [0, 1]$. In FFR we employ a CC reuse factor of $\Delta_c = 1$, and CE reuse factor of $\Delta_e > 1$, with Δ_e number of cells participating in resource allocation to the CE. It is important to mention here that due to the varying demands of users it is highly probable that each of the i th cell in the cluster of Δ_e number of cells i.e., $i \in \{1, 2, \dots, \Delta_e\}$, has a different threshold radius r_{n_i} . Therefore, for the performance computation and comparison we consider Δ_e reference users for each of the CC and CE region in polar coordinates located at (r_i^c, θ_i^c) and (r_i^e, θ_i^e) respectively. Every reference user is served by a reference BS which is nearest to it and the interfering BSs employing the same sub-band as shown in Fig. 1a.

2.1 Strict FFR

Strict FFR considered in [5] assumes same deployment scenario for all cells in the cluster giving rise to the same threshold radius for cell partitioning i.e. $r_{n_1} = r_{n_2} = \dots = r_{n_{\Delta_e}}$. Hence, equally dividing the bandwidth into Δ_e cells with equal geographical areas of CE regions. Usually, no power control is used in strict FFR scheme and equal power allocation (EPA) on all sub-bands (or sub-carriers) is employed [5,8].

2.2 Channel model and SINR

The channel in a typical fading environment consists of path-loss, small-scale fading, and shadowing. For the ease of analysis, channel under consideration consists of small-scale fading following Rayleigh distribution and the path-loss

while shadowing is ignored as it can be easily overcome via power control over the fading-time [34]. Let the transmit power be P_T for all BSs, then the received power P_R at a mobile user from the BS can be modeled as the product of path-loss component L and the power of fading gain ζ as

$$P_R = P_T L \zeta. \tag{1}$$

Path-loss L is modeled as $L = kd^{-\alpha}$ [35], where $k = (\lambda/(4\pi))^2$ is the free-space path-loss at a reference distance of 1m depending upon the wavelength λ , d is the distance between the BS and the mobile user, and α is the path-loss exponent. Since, Rayleigh distribution is considered for channel gain, its power ζ follows exponential distribution [36] with parameter μ i.e. $\zeta \sim \exp(\mu)$. Let us consider the transmit power of BSs to be $P_T = 1/\mu$. The received SINR at the reference user u_i of the i th cell can be expressed as

$$\gamma_i = \frac{P_{T_i} L_i \zeta_i}{\sum_{j \in J_i} P_{T_j} L_j \zeta_j + \sigma_N^2}, \tag{2}$$

where j th interfering BS belongs to J_i ; the set of interferers for every reference user u_i , σ_N^2 is the power of noise which is considered to be additive and constant here. Slight modification of (2) results in the following expression for the received SINR

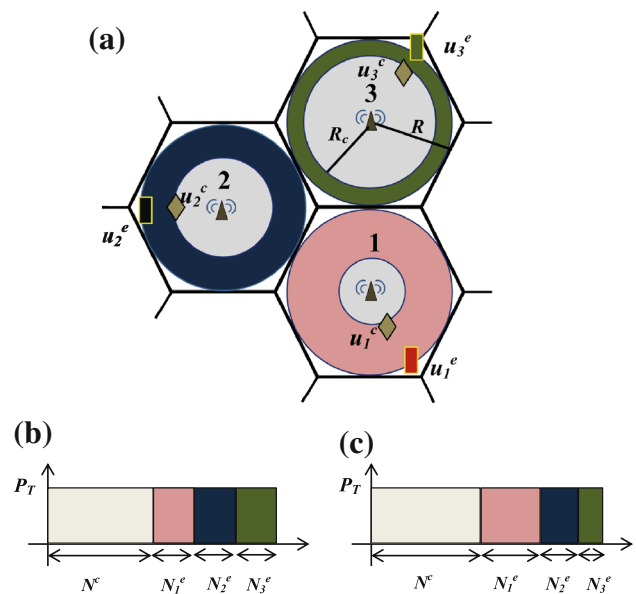


Fig. 1 3-cell cluster in which CC reference mobile users (u_i^c) are shown with a diamond symbol while CE users (u_i^e) are indicated by rectangular boxes in the three reference cells; **a** illustration of cells with different radii for CC and CE area, **b** fixed frequency allocation in strict FFR, and **c** proposed dynamic frequency allocation for CE users

$$\gamma_i = \frac{L_i \zeta_i}{\sum_{j \in J_i} L_j \zeta_j + g} \tag{3}$$

where (3) follows from EPA to all sub-bands with $g = 1/SNR = \mu\sigma_N^2$ being the reciprocal of signal-to-noise power ratio (SNR).

2.3 Distance between reference user and interfering BSs

Since, the path-loss L_j is a function of the distance between the i th reference user and the j th co-channel interfering BS in the list J_i , therefore it is required to properly calculate the distances $d_{i,j}$ between an i th reference user and j th interferer. A common approach for polar coordinate system is to employ law of cosines given as

$$d_{i,j} = \sqrt{D_{i,j}^2 + d_i^2 - 2 D_{i,j} d_i \cos \theta_{i,j}}, \tag{4}$$

where $D_{i,j}$ is the distance between the i th reference BS and the j th interfering BS, d_i is the distance of reference user from its corresponding nearest BS, and $\theta_{i,j}$ is the angle between user and the corresponding interferer. As evident from Fig. 2, the angle $\theta_{i,j}$ is not known to the centralized controller directly and is calculated with simple algebraic manipulation.

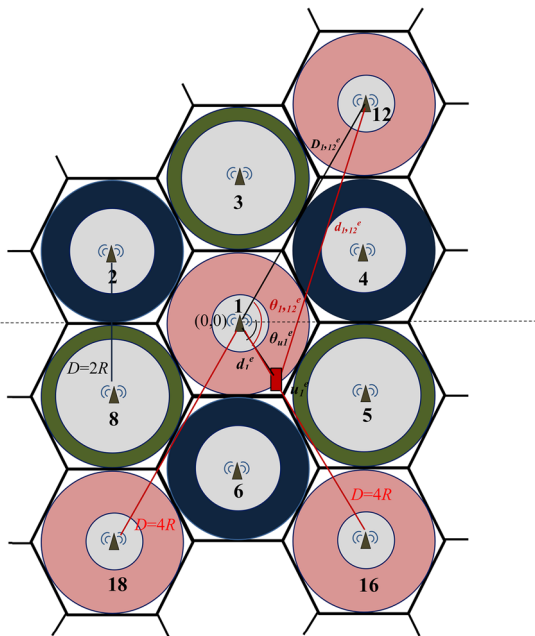


Fig. 2 Distance between reference user u_1^e and 12th interfering BS. The inter-BS distance $D_{1,12} = 4R$. Reference user is at a distance $d_1 = R$

3 Proposed bandwidth partitioning algorithm

Here we consider cluster of 3 cells $i \in \{1, 2, 3\}$ because it is the optimal and most widely used CE reuse factor [16]. But, the proposed dynamic bandwidth partitioning scheme can quite conveniently be extended to the cluster of 7 cells. The cells are monitored on the basis of received SINR and the number of users in CC region to quantify the distance threshold r_{ni} . We assume different threshold radii within the cluster and repeated cluster patterns due to FFR consideration as depicted in Fig. 3. For the purpose of analyzing the scheme user distribution is still uniform in every cell; only the intensity is varying allowing the corresponding cell to partition the cell and resource according to its own demands. The proposed work considers the full frequency reuse for CC regions ($\Delta_c = 1$) which means that all the considered cells with different demands use the same sub-band for the CC users. Lets say we have N total sub-carriers. The proposed way out is to find N_c sub-bands firstly depending upon every cell’s center area and the reuse factor (Δ_e), and then consider its average to be used by every cell. Every i th BS can determine this partitioning radius that maximizes the SE of the cell and can share this information with the central coordinator i.e. radio network controller (RNC). This cooperative communication is performed via the wired back haul (X2 interface) connecting the BSs to a common RNC and hence no other means of communications are needed. The main contribution of RNC is to manipulate the data from different BSs in a centralized fashion as described by the Algorithm 1 for the allocation of resources. Determining the appropriate FRF for CE (Δ_e) defines the number of interferers J_i , and hence, every BS computes the interferer distance, path-loss and spectral efficiency for its reference user. Once this data is collected, the controller allocates the resources by following either Algorithm 2 or Algorithm 3. Whenever user demands or user distributions change, BSs update their r_{ni} and RNC applies the proposed allocation algorithm again. Performance metrics are also computed again. This is how the dynamics of traffic demands are handled. Fig. 1b, c visualize how the bandwidth is partitioned in static FFR schemes and the dynamic scheme favoring the CE users respectively.

3.1 Fixed allocation of resources

Algorithm 2 describes the fixed allocation of resources. For every cell the center band is allocated proportional to the average demands of cells i.e. A_{avg}^c . Once the sub-band N^c is allocated, the essence of fixed allocation is to divide the remaining portion equally among the Δ_e number of cells as is done for equal radii of cells in [5].

Algorithm 1 Centralized data manipulation

Input: $f_c, SNR, \alpha, N, D_{i,j}, d_i$ // System Parameters, inter-BS distances and user locations
 1: Determine Δ_c and Δ_e .
 2: **for** $i = 1 : \Delta_e$ **do**
 3: Determine threshold radii r_{ni} and interferer sets J_i
 4: **for** $m \in \{c, e\}$ **do**
 5: Determine reference user u_i^m locations (d_i^m, θ_i^m) // considering worst-case user with highest ICI
 6: Calculate distances $d_{i,j}^m$ using (4) // the distance between j-th interferer and reference user u_i^m
 7: Calculate path-losses L_i^m and L_j^m // as detailed in Sect. 2.2
 8: Assign N_i^m according to Algorithm 2 or 3
 9: Calculate the capacities C_i^m and ASE_i^m // as detailed in Sect. 4
 10: **end for**
 11: **end for**
Output: $r_{ni}, d_{i,j}, N_i^c, N_i^e, L_i, L_j, C_i^c, C_i^e, ASE^c, ASE^e$ // Performance Metrics

Algorithm 2 Fixed allocation of resources to the CE

Input: r_{ni}, Δ_e, N
 1: $\xi = \sum_{i=1}^{\Delta_e} r_{ni}^2$ // sum of normalized center region areas
 2: $\mathcal{A}_{avg}^c = \frac{\xi}{\Delta_e}$
 3: $N^c = \mathcal{A}_{avg}^c$ // Average demand satisfaction for CC regions
 4: $N^e = N - N^c$
 5: **for** $i = 1$ to Δ_e **do**
 6: $N_i^c = N^c$
 7: $N_i^e = \frac{N^e}{\Delta_e}$ // equal partitioning for edge users
 8: **end for**
Output: N^c, N^e, N_i^c, N_i^e

3.2 Proposed centralized dynamic allocation of resources

The proposed allocation scheme described in Algorithm 3 aims at improving both the CC and CE performance by allocating more resources to the CC region than the fixed one depending upon cell partitioning and dynamic allocation to CE regions considering the demands of the individual cells. If two or more cells have CC areas exceeding their respective CE areas, all CC regions are allocated bands proportional to the maximum normalized CC area; \mathcal{A}_{max}^c . Lines 8 till 11 of Algorithm 3 demonstrate this allocation. Variable ind is an array that records the indices of cells with CC areas greater than CE areas i.e. $r_{ni} > 0.5$. If this condition is not true, CC resource portion N^c is average CC area-based allocation plus finer allocation. This finer allocation factor Ψ depends upon the center areas of Δ_e number of cells and benefits the cells with higher CC area that are under allocated. The proposed allocation scheme for CC areas seems to over-allocate the cell with $r_{ni} < 0.5$ and hence, a smaller portion of bandwidth would be left for CE allocation. This constraint

is managed by proportional allocation to CE areas as well. Weight factors proportional to the CE area, w_i , are utilized for partitioning of edge band N^e into individual CE sub-bands N_i^e . This weighted-resource partitioning takes much care of the demands of the cells. Existence of many competent dynamic algorithms motivates for the *complexity analysis* of our algorithm. The proposed algorithm performs Δ_e number of iterations twice and a search operation on the same Δ_e number of participating cells. These resource allocation operations have complexity order $\mathcal{O}(\Delta_e)$. Therefore, complexity order of the proposed algorithm is $\mathcal{O}(\Delta_e)$, that is *linear* complexity.

Lets elaborate the proposed allocation scheme by considering the following two scenarios; scenario 1 as [$r_{n1} = 0.3, r_{n2} = 0.6, r_{n3} = 0.8$] and scenario 2 as [$r_{n1} = 0.5, r_{n2} = 0.9, r_{n3} = 0.4$]. These are worst-case scenarios i.e. for fully loaded cells and are considered for better elaboration of resource allocation schemes. In-depth overview of proposed schemes is provided by 3D plots discussed in Sect. 5. For scenario 1, since two cells have $r_{ni} > 0.5$, therefore $N_d^c = \mathcal{A}_{max}^c$ which is \mathcal{A}_3^c . CC region of cell 1 is over allocated but its CE must be allocated the largest portion amongst other cells. Thus not only the CC spectral efficiency (SE) will improve, but CE SE will also, thereby improving the overall ASE. For the second scenario, average allocation suffices but finer allocation benefits CC region of cell 2. With this more portion a smaller N^e is available. Proportional weighted allocation here works well by providing N_3^e the most portion.

DFFR [21] assigns resources to CC and CE users similar to strict FFR studied in Algorithm 2 under normal traffic conditions. A portion, η percentage, of CE resource is kept shared amongst cluster cells. When a cell with huge data demand emerges, these shared resources are allocated to it in order to meet CE user demands.

4 Area spectral efficiency analysis

ASE is a performance metric measured as the SE per unit cell area (bps/Hz/cell/km²) while considering areas in km² and is widely used in literature [5,37,38]. Considering the normalized cell area and sub-carrier allocations for every i th cell in the cluster, its ASE (bps/Hz/km²) is given by

$$ASE_i = \underbrace{\frac{N_i^c}{N} \mathcal{A}_i^c C_i^c}_{\text{CC component}} + \underbrace{\frac{N_i^e}{N} \mathcal{A}_i^e C_i^e}_{\text{CE component}}, \tag{5}$$

where $N = N^c + \sum_i N_i^e$ is the total number of available sub-carriers, and C_i^c and C_i^e are the achievable capacities per Hz (bps/Hz) for the CC and CE of the considered cell respectively. The sub-carriers for CC and CE areas (N_i^c and

Algorithm 3 Proposed dynamic allocation of resources to the CE

Input: $r_{n_i}, \Delta_c, \Delta_e, N$
 1: **initialize:** $N_d^c \leftarrow N_s^c // N_s^c$ is N^c of Algorithm 2
 2: $\xi = \sum_{i=1}^{\Delta_e} r_{n_i}^2 //$ sum of normalized center region areas
 3: **for** $i = 1$ to Δ_e **do**
 4: $\mathcal{A}_i^c = r_{n_i}^2 //$ normalized center region area for cell i
 5: **end for**
 6: $\Phi = \min(\mathcal{A}_1^c, \mathcal{A}_2^c, \dots, \mathcal{A}_{\Delta_e}^c)$
 7: $\Psi = \frac{\Phi}{\xi \Delta_e (\Delta_e - \Delta_c)} //$ finer allocation factor
 8: $\mathcal{A}_{max}^c = \max(\mathcal{A}_1^c, \mathcal{A}_2^c, \dots, \mathcal{A}_{\Delta_e}^c)$
 9: $ind = \text{find}(r_{n_i} > 0.5)$
 10: **if** ($\text{length}(ind) > 1$) **then**
 11: $N_d^c = \mathcal{A}_{max}^c$
 12: **else**
 13: $N_d^c = N_d^c + \Psi$
 14: **end if**
 15: $N_d^e = N - N_d^c$
 16: **for** $i = 1$ to Δ_e **do**
 17: $N_i^c = N_d^c$
 18: $\mathcal{A}_i^e = 1 - \mathcal{A}_i^c //$ Normalized edge region area for cell i
 19: $\omega_i = \frac{\mathcal{A}_i^e}{\Delta_e - \xi} //$ factor proportional to demand of cell i
 20: $N_i^e = \omega_i N_d^e$
 21: **end for**
Output: $N_d^c, N_d^e, N_i^c, N_i^e$

N_i^e) are determined from the algorithms provided in the previous section. It can be noted from (5) that total ASE of cell comprises of SE of CC and CE regions, therefore the total ASE (ASE_T) of a cluster of cells is given by

$$ASE_T = \sum_{i=1}^{\Delta_e} ASE_i. \tag{6}$$

In (5), the normalized CC and CE areas are $\mathcal{A}_i^c = r_{n_i}^2$ and $\mathcal{A}_i^e = 1 - r_{n_i}^2$, respectively for every $i \in \{1, 2, \dots, \Delta_e\}$.

4.1 Capacity calculations

The Shannon capacity [39] for fading interference channel as a function of SINR γ is generally given as

$$C = \mathbb{E}[\log_2(1 + \gamma)]. \tag{7}$$

The capacity for i th cell can therefore be written as a function of SINR γ_i as follows

$$C_i = \mathbb{E}[\log_2(1 + \gamma_i)]. \tag{8}$$

Substituting SINR expression from (3) in (8) results in

$$C_i = \mathbb{E} \left[\log_2 \left(1 + \frac{L_i \zeta_i}{\sum_{j \in J_i} L_j \zeta_j + g} \right) \right] = \mathbb{E} \left[\log_2 \left(1 + \frac{k d_i^{-\alpha} \zeta_i}{\sum_{j \in J_i} k d_{i,j}^{-\alpha} \zeta_j + g} \right) \right], \tag{9}$$

where J_i is the set containing interferers for reference user in i th cell. From Fig. 3 the interferers J_i for u_i^c in the CC, J_i^c , are all the BSs other than the i th BS and for u_i^e in the CE are $J_1 = \{8, 10, 12, 14, 16, 18\}$, $J_2 = \{4, 6, 11, 15, 19\}$ and $J_3 = \{5, 7, 9, 13, 17\}$ for $i = 1, 2, 3$.

Since (9) comprises of a large number of random variables whose expectation can not be easily computed for capacity calculation, therefore we utilize the lemma presented in [40] and the moment generating function (MGF) based approach for J number of i.i.d. Rayleigh distributed interferers. Performing these steps, the capacity can be calculated as

$$C_i = \log_2 e \int_0^\infty \frac{1}{z} \left(1 - \frac{1}{1 + z L_i} \right) \prod_{j \in J_i} \left(\frac{1}{1 + z L_j} \right) e^{-z g} dz. \tag{10}$$

Reader may refer to the appendix for detailed calculation. This expression contains only a single integral which can easily be solved using numerical methods unlike the approach of finding PDF expression for SINR and then averaging it over a given area of CC or CE [41]. ASE for a given cell i can be computed by finding the capacities for CC and CE i.e., C_i^c and C_i^e respectively via (10), when reference users u_i^c and u_i^e are taken into consideration.

5 Results and discussion

In this section, the proposed dynamic resource allocation scheme is analyzed for a hexagonal grid of 19 cells. The FRF of $\Delta_c = 1$ and $\Delta_e = 3$ are considered giving rise to 3 reference cells with reference users located at locations $u_1^e : (R, 300^\circ)$, $u_2^e : (R, 180^\circ)$ and $u_3^e : (R, 60^\circ)$ for the CE regions and $u_1^c : (r_{n_1} R, 300^\circ)$, $u_2^c : (r_{n_2} R, 165^\circ)$ and $u_3^c : (r_{n_3} R, 75^\circ)$ for the CC regions with the reference BS-1 located at the origin. Under this scenario, the interferer sets for CE are $J_1^e = \{8, 10, 12, 14, 16, 18\}$, $J_2^e = \{4, 6, 11, 15, 19\}$ and $J_3^e = \{5, 7, 9, 13, 17\}$ and for CC region the interferers are the set of all BSs other than the reference BS. Various system parameters along with their values

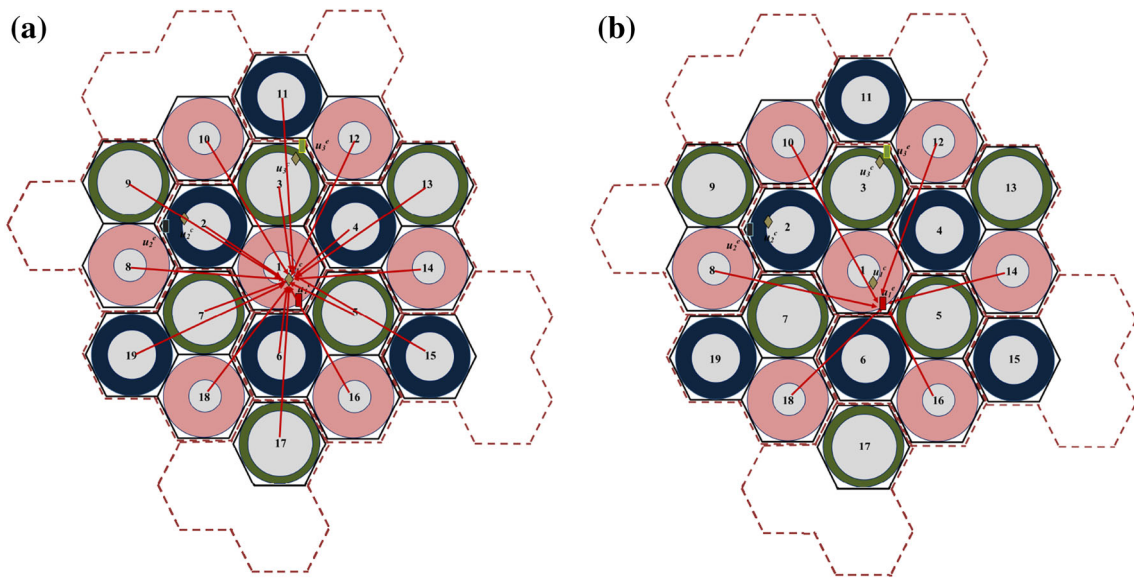


Fig. 3 The network under consideration consists of 19 BSs with 3 reference cells and the co-channel interference signals shown with red arrows: **a** the CC reference user for cell 1 is located at $(R_{c1}, 180^\circ)$ where

R_{c1} indicates the CC radius, and **b** the CE reference user is located at $(R, 180^\circ)$ where R is the cell radius

Table 1 System Parameters

Parameter	Value
Carrier frequency f_c	70, 700 MHz
Cell radius R	1 km
Normalized center radius r_n	Varies between [0, 1]
Path-loss exponent α	3, 4
Antenna configuration	SISO
FRF for CC users Δ_c	1
FRF for CE users Δ_e	3
SNR	Varies between [-10, 60]
Available sub-carriers N	Normalized to 1
Macro-cell BS transmit power P_T	1

are listed in Table 1. System level simulations are performed with the aid of numerical methods using MATLAB. These results compare the proposed scheme with reference fixed allocation scheme via ASE and SE (area averaged) under various design parameters.

The proposed scheme is compared with the fixed allocation in strict FFR in Figs. 4 and 5 under different values of path loss exponent and carrier frequency. It is observed that the increase in path loss exponent leads to more power degradation in both desired signal and interference signal. Also the increase in f_c implies reduced k factor and hence more performance degradation.

ASE analysis of the proposed scheme in terms of normalized total ASE is presented in Fig. 6 for the two scenarios.

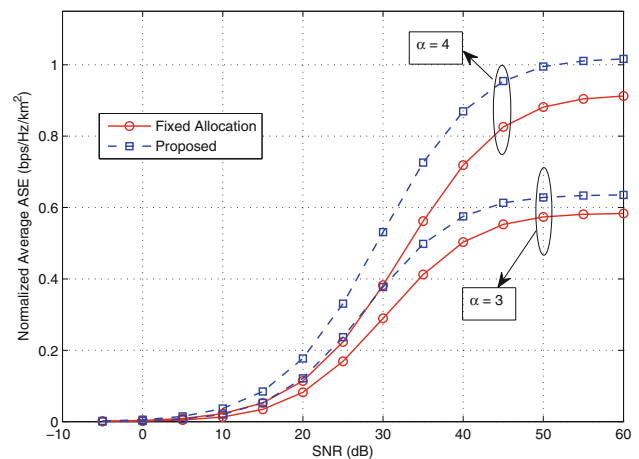


Fig. 4 Normalized average ASE over the cluster of 3 cells against SNR for the strict FFR and the proposed scheme with the path-loss exponent of 3 and 4 and cell radii: $[r_{n1} = 0.3, r_{n2} = 0.6, r_{n3} = 0.8]$

The nature of curves is an evidence of logarithmic dependence of capacity on SNR. The performance gain is high for SNR exceeding 20 dB. The gain is observed to follow logarithmic trend and is found to be about 18 and 8% for scenario 1 and 2 respectively at SNR of 60 dB. Maximum gain is observed to be 30% at SNR of 35 dB. Scenario 1 shows improved overall ASE and performance gain than the scenario 2.

Total SE of CC and CE regions of the proposed scheme are illustrated in Figs. 7 and 8 respectively. It can be observed that the scenario 1 has higher SE for CC and reduced SE for CE

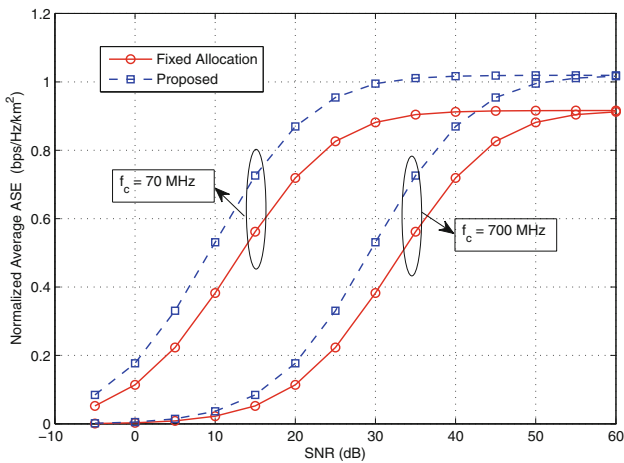


Fig. 5 Normalized average ASE against SNR for the strict FFR and the proposed scheme under varying carrier frequency with cell radii: $[r_{n1} = 0.3, r_{n2} = 0.6, r_{n3} = 0.8]$

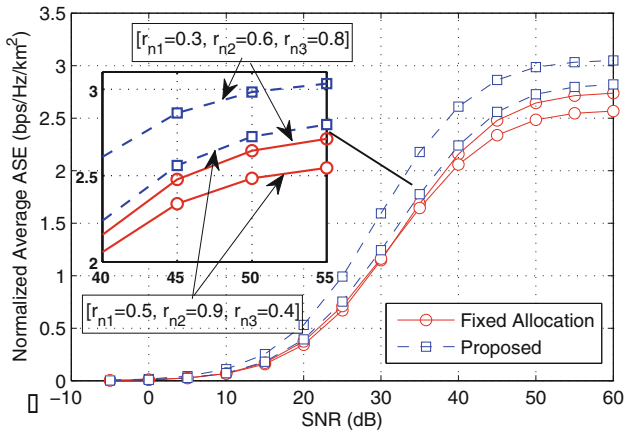


Fig. 6 Total ASE for 3 cells against SNR comparing the strict FFR and the proposed scheme with $\alpha = 4$, $f_c = 700$ MHz and the cell-radii as shown

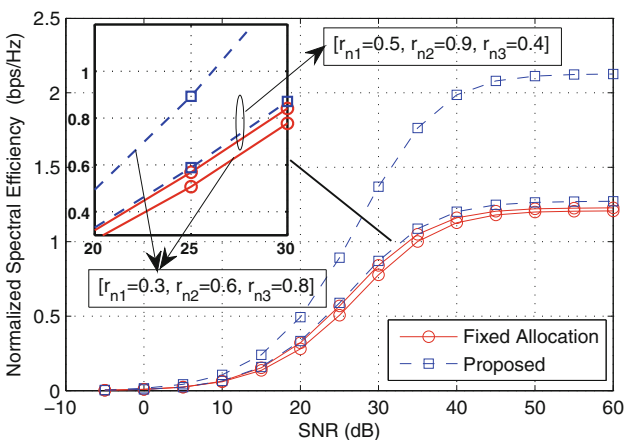


Fig. 7 Total SE for 3 cells' center regions against SNR comparing the strict FFR and the proposed scheme under the two scenarios

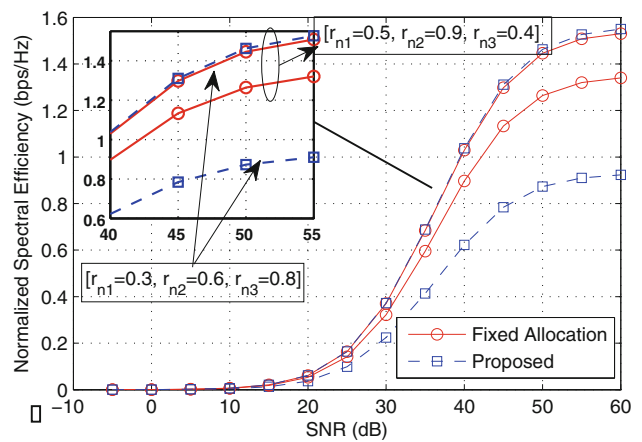


Fig. 8 Total SE of 3 cells' edge regions of the proposed scheme under the two scenarios

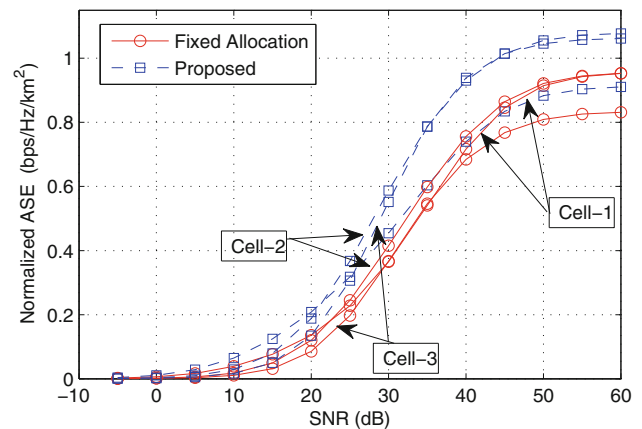


Fig. 9 ASE for 3 cells against SNR comparing the strict FFR and the proposed scheme with cell radii: $[r_{n1} = 0.3, r_{n2} = 0.6, r_{n3} = 0.8]$

while the opposite holds for scenario 2. Performance gains for scenario 2 are better for both CC and CE giving higher overall performance gain as evident from Fig. 6. For scenario 1, a huge portion of total band goes to CC area leaving a smaller portion for CE region users. Since, SE varies directly with allocated bandwidth, CC SE of the proposed scheme under scenario 1 is quite larger than the fixed scheme. In case of edge allocation we see a similar decline in SE of the proposed scheme as compared to fixed scheme. However, this overall decrease is compensated by prioritizing the cells with higher CE areas.

Figures 9 and 10 visualize the total ASEs of 3 cells under scenario 1 and 2 respectively as a function of SNR. The ASE for a given cell comprises of the SE of CC and CE regions. It can be observed that the SE of CC region is quite higher than the SE of CE region, therefore the ASE behavior is coincident with that of CC SE which is proportional to the area covered as depicted by Figs. 11 and 13. In scenario 1,

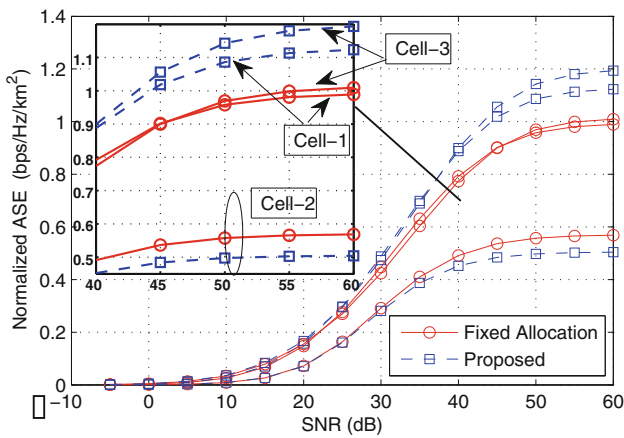


Fig. 10 ASE for 3 cells against SNR comparing the strict FFR and the proposed scheme with cell radii: $[r_{n_1} = 0.5, r_{n_2} = 0.9, r_{n_3} = 0.4]$

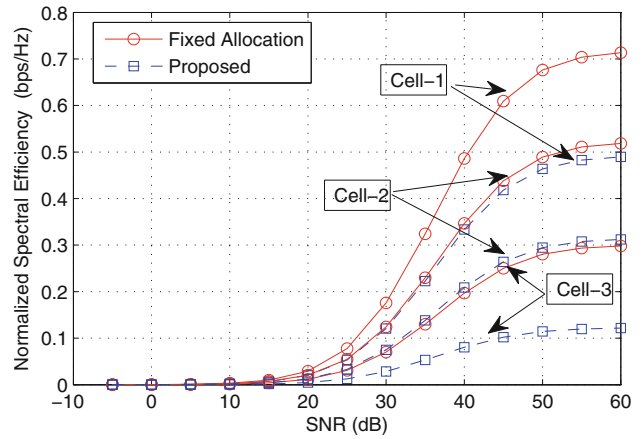


Fig. 12 SE for 3 cells' edge region against SNR with cell radii: $[r_{n_1} = 0.3, r_{n_2} = 0.6, r_{n_3} = 0.8]$

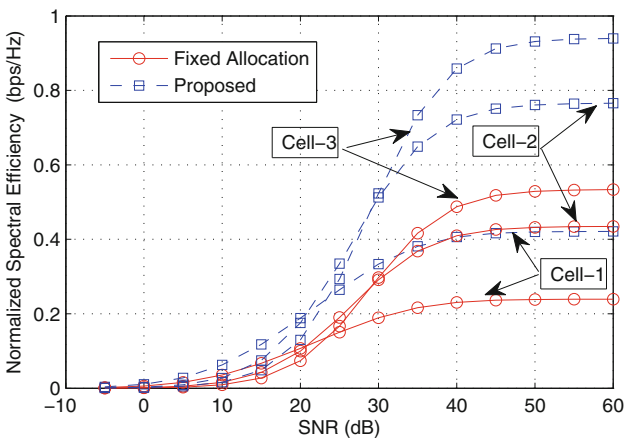


Fig. 11 SE for 3 cells' center region against SNR with cell radii: $[r_{n_1} = 0.3, r_{n_2} = 0.6, r_{n_3} = 0.8]$

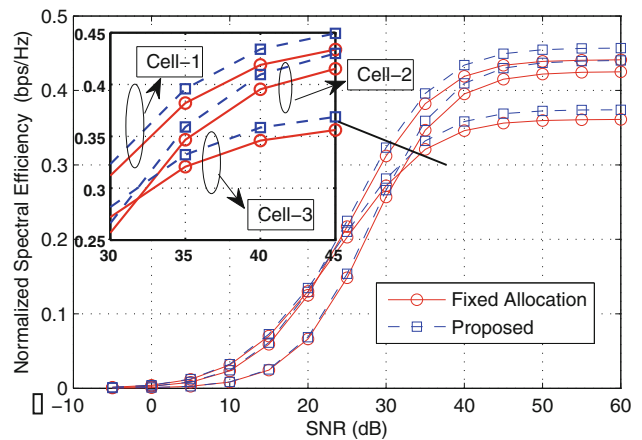


Fig. 13 SE for 3 cells' center region against SNR with cell radii: $[r_{n_1} = 0.5, r_{n_2} = 0.9, r_{n_3} = 0.4]$

the CC areas are $\mathcal{A}_3^c > \mathcal{A}_2^c > \mathcal{A}_1^c$ and so are the ASEs as shown in Fig.9. Increasing normalized radius increases the bandwidth portion being allocated and hence an increased ASE performance. Fig.10 indicates the ASE performances proportional to CC areas which are $\mathcal{A}_2^c > \mathcal{A}_1^c > \mathcal{A}_3^c$ or $\mathcal{A}_1^c \approx \mathcal{A}_3^c$ for scenario 2.

Per-cell performance in terms of SE as a function of SNR is compared with the 3 cells for the scenario 1's CC and CE regions in Figs.11 and 12 respectively, and for scenario 2's CC and CE regions in Figs.13 and 14 respectively. The proposed area based allocation to the CC improves the overall as well as the per cell SE performance. This is because every cell is allocated a band that satisfies the average demands of CC region users of all cells better than the strict FFR fixed allocation. This allocation of average CC demand satisfaction implies from the priority given to CE users here in this scheme and satisfaction of average demands of CC users is taken into account. More number of users imply shrinkage of CC radius r_{ni} [7]. From the obtained results, the cell with higher

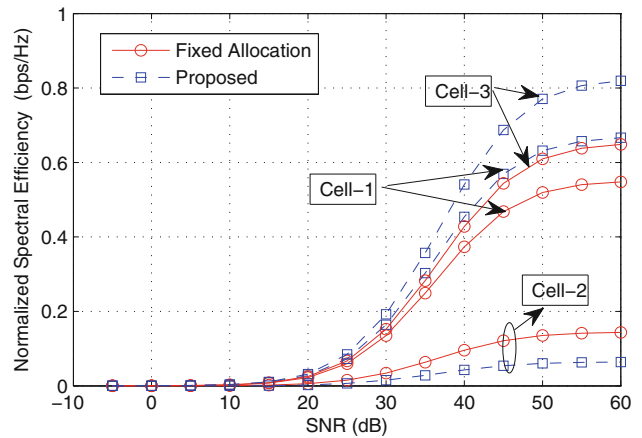


Fig. 14 SE for 3 cells' edge region against SNR with cell radii: $[r_{n_1} = 0.5, r_{n_2} = 0.9, r_{n_3} = 0.4]$

concentration of users in CC implying reduced r_{ni} has poor CC SE performance and better CE SE performance because of the fact that the resources are proportionally allocated.

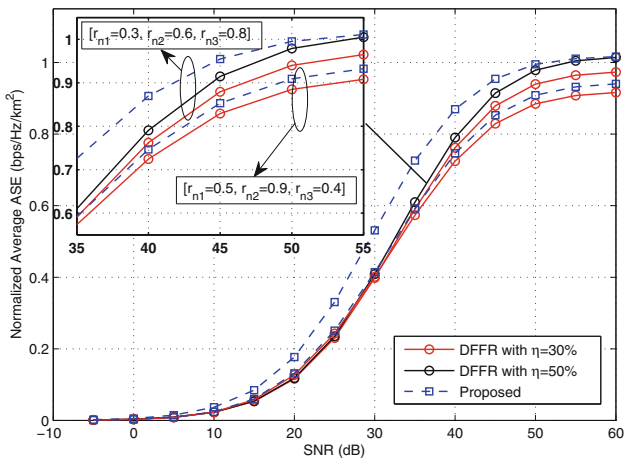


Fig. 15 Average ASE against SNR comparing the DFFR and the proposed scheme for the cell-radii as shown

Due to centralized allocation, no cell with heavy data demand will be suffering from poor ASE. The cells with low demands or higher r_{ni} seem to suffer as compared to the static allocation, nonetheless, these cells already get most of the user’s demands satisfied in CC region as their radii contribute a significant portion in average resource to all cell’s center region. CE user performance is better for the cell with higher CE area (lower value of r_n), e.g. the cell 1 for scenario 1.

Lets compare the average normalized ASEs of proposed scheme and DFFR for the two scenarios. In Fig. 15, proposed scheme outperforms DFFR with $\eta = 30\%$ as well as with $\eta = 50\%$. Increasing the shared resource percentage η increases the ASE performance [21]. This increase is more evident at high SNR values. However, this huge percentage of shared band means a smaller portion being left for allocation to other cells of cluster and hence their reduced SEs. Maximum gain for ASE performance in Fig. 15 is close to 30% for $\eta = 50\%$ and 23% for $\eta = 30\%$ for scenario 1 and about 3% for scenario 2.

Lets now consider scenario 2 i.e. ($r_{n1} = 0.5, r_{n2} = 0.8$ and $r_{n3} = 0.4$) for spectral efficiency analysis comparison. Sharing factor η is fixed to 30%. SEs for three cells’ CC and CE regions in Figs. 16 and 17 follow the same trends as discussed in Figs. 13 and 14 respectively. Proposed scheme shows better performance than DFFR for all cells’ CC regions. CE spectral efficiencies however behave interestingly. DFFR allocates all $\eta\%$ resources to the edge region of cell with maximum demand i.e. cell 3 in our case. We can see DFFR’s performance overshoot for cell 3 in Fig. 17. Proposed scheme shows good performance for cell 2 and tolerable performance for cell 1. Proposed scheme seems to be in trouble. Fig. 18 provides best picture in this regard. Overall average SE for CE region is still votes for proposed scheme. This is because of the tradeoff among allocation to one cell

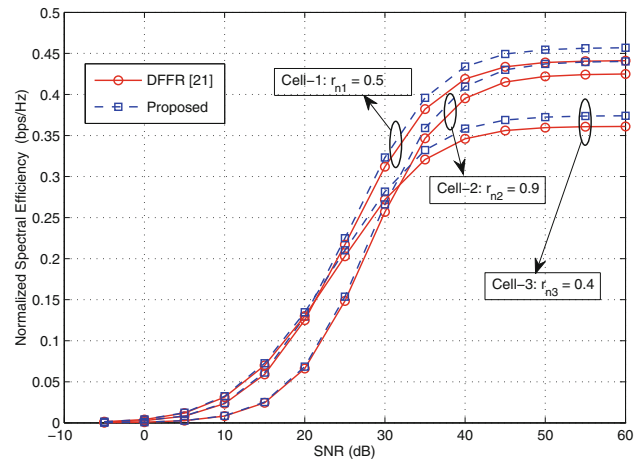


Fig. 16 Average SE against SNR comparing the DFFR and the proposed scheme for CC regions of shown cell-radii

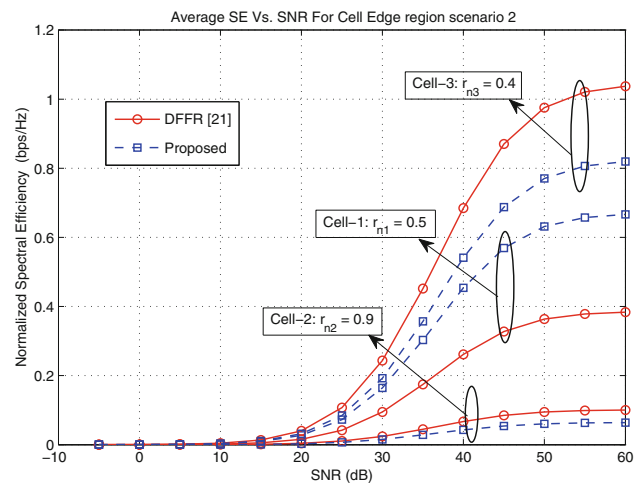


Fig. 17 Average SE against SNR comparing the DFFR and the proposed scheme for CE regions of shown cell-radii

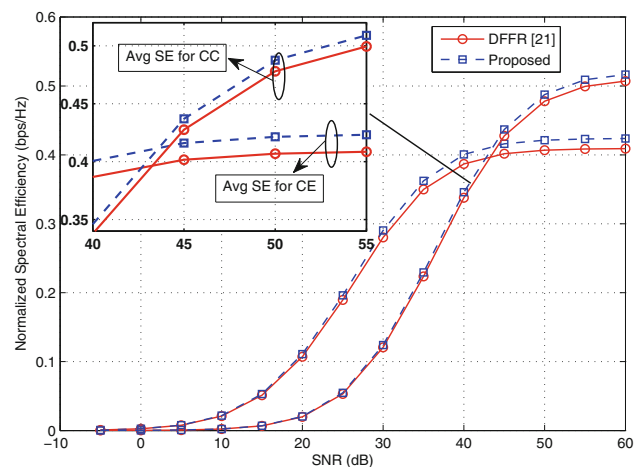


Fig. 18 Average CC and CE SE against SNR comparing the DFFR and the proposed scheme

Fig. 19 SE for CC and CE regions from three-dimensional viewpoint; two cell radii are fixed to $r_{n_2} = 0.2$ and $r_{n_3} = 0.7$ while varying the radius of cell 1 r_{n_1} and sub-carriers allocated to it (N_1^e)

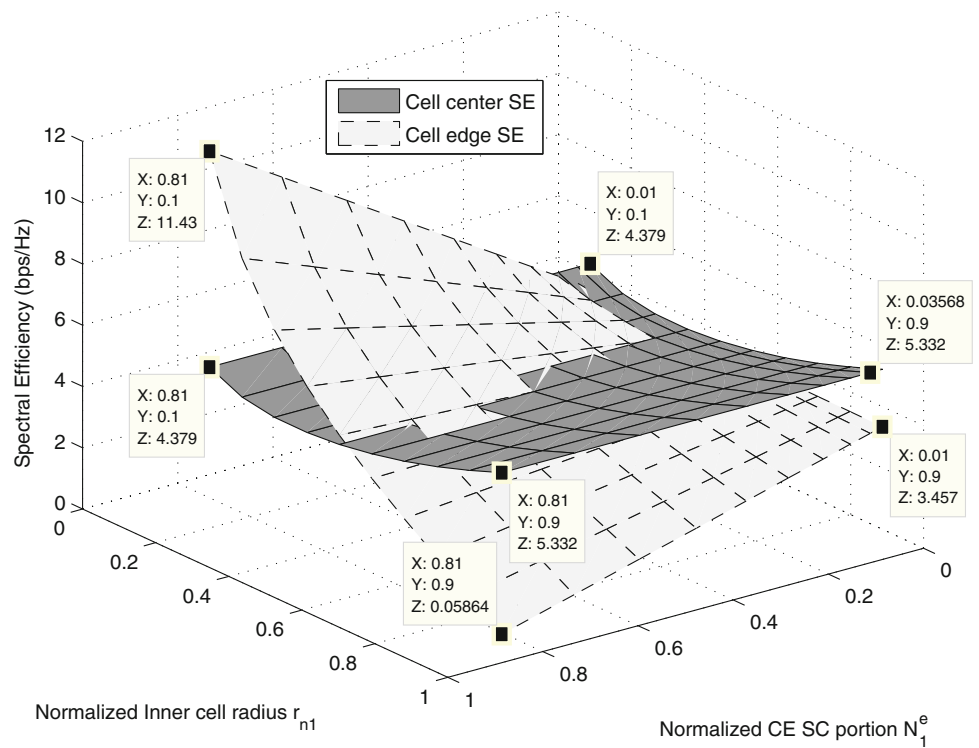
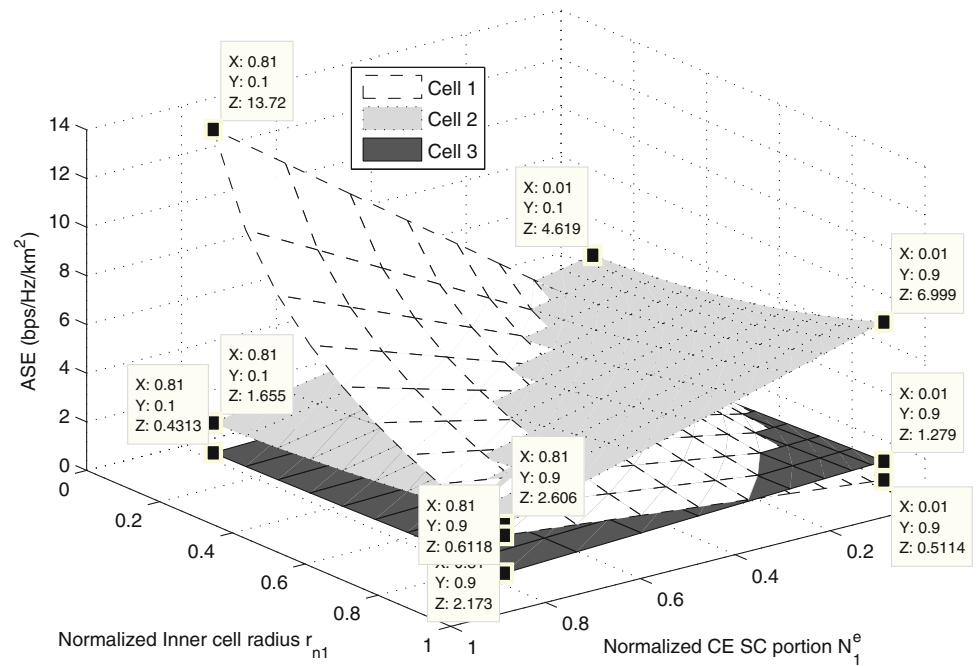


Fig. 20 ASE from three-dimensional viewpoint for 3 cells; two cell radii are fixed to $r_{n_2} = 0.2$ and $r_{n_3} = 0.7$ while varying the radius of cell 1 r_{n_1} and sub-carriers allocated to it (N_1^e)



and the remaining band at hand for other cells of cluster. DFFR takes good care of cell 3's edge region, rather it is over-allocated, but cell 1 and cell 2 remain under-allocated. Proposed scheme however keeps a balance by proportionally allocating all CE regions.

To get more insights of the proposed scheme, 3D plots of SE and ASE are presented in Figs. 19 and 20 respectively. The existing tradeoff for CC and CE performance is

observed as analyzed in [8] for two scheduling schemes. 3D plot of ASE shows the performance change of cell-1 when its radius threshold and hence the sub-carriers allocated to it are changed while the other cells keep their demands constant. We observe that increase in CC radius leads to increased CC SE but reduced CE SE. As already stated, this is due to increased CC allocated sub-carriers. However, we are eventually left with a smaller portion for CE users N^e and a

decreasing CE SE. For a given CC radius, CE sub-carrier partitioning largely impacts the CE SE. ASE is largely affected by spectrum partitioning. Lets see the impact of cell 1’s CC radius variations on individual cell ASEs. Initially when $r_{n_1} < r_{n_2} < r_{n_3}$ and N_1^e is quite large (say, close to 0.8), ASE of cell 1 overshoots the other cells’ ASEs. When this distance threshold increases, CC SE portion increases and ASEs of cell 2 and cell 3 increase with the given SE for cell 1. As N_1^e eventually decreases, ASE performance for cell 1 becomes poor.

6 Conclusions

A centralized dynamic resource allocation scheme is presented in this paper. The scheme allocates more sub-carriers to the CC users as compared to the average demand satisfaction based fixed allocation scheme while CE users are proportionally taken care of. Complexity analysis is provided as a metric for practicality of the proposed algorithm. We compare the proposed resource allocation scheme with strict FFR and DFFR. The scheme shows performance improvements for CC as well as CE users with an overall normalized ASE improvement of up to 30%. Various existing trade-offs among CC and CE users are also observed. This inter-dependency of cells for resource allocation and ASE performance is well depicted by three-dimensional ASE plots.

Appendix

Proof of capacity expression in (10) follows from the lemma presented in [40] stated as

$$\ln(1 + x) = \int_0^\infty \frac{1}{s} (1 - e^{-sx}) e^{-s} ds, \forall x \geq 0 \tag{11}$$

and the fact that

$$\log_2 x = \log_2 e \cdot \ln x. \tag{12}$$

Lets represent the capacity to be of the form

$$C = \log_2 \left(1 + \frac{X}{\sum I + g} \right), \tag{13}$$

where $X = L_i \zeta_i$ is the signal component and $I = \sum_{j \in J_i} L_j \zeta_j$ is the interference component (the CCI). Substituting $s = z (\sum I + g)$ in (11), and using (12), we have

$$\begin{aligned} \log_2 1 + \frac{X}{\sum I + g} \\ = \log_2 e \int_0^\infty \frac{1}{z} (1 - e^{-zX}) e^{-z \sum I} e^{-zg} dz. \end{aligned} \tag{14}$$

Taking the $\mathbb{E} [\cdot]$ on both sides of (14), gives the capacity based on the MGF-approach as

$$C = \log_2 e \cdot \int_0^\infty \frac{1}{z} (1 - \mathcal{M}_{\mathcal{X}}(z)) \mathcal{M}_{\mathcal{I}}(z) e^{-zg} dz, \tag{15}$$

where $\mathcal{M}_{\mathcal{X}}(z) = \mathbb{E} [e^{-zX}]$ and $\mathcal{M}_{\mathcal{I}}(z) = \mathbb{E} [e^{-zI}]$ are the MGFs of the useful signal X and interfering signal I respectively. MGFs have the property that the expectation of a sum of RVs can be represented as a product of their expectations when the RVs are assumed to be independent of each other [42]. Using this fact and [36], the MGFs for i.i.d. Rayleigh distributed interferers ($\zeta \sim \exp(\mu)$) can be computed as follows

$$\mathcal{M}_{\mathcal{X}}(z) = \mathbb{E} [e^{-zL_i \zeta_i}] = \frac{1}{1 + zL_i}. \tag{16}$$

$$\mathcal{M}_{\mathcal{I}}(z) = \prod_{j \in J_i} \mathbb{E} [e^{-zL_j \zeta_j}] = \prod_{j \in J_i} \frac{1}{1 + zL_j}. \tag{17}$$

Substituting the MGFs from (16) and (17) in (15) gives the capacity formula in (10).

References

1. Boudreau, G., Panicker, J., Guo, N., Chang, R., Wang, N., & Vrzic, S. (2009). Interference coordination and cancellation for 4 G networks. *IEEE Communications Magazine*, 47(4), 74–81.
2. Hamza, A. S., Khalifa, S. S., Hamza, H. S., & Elsayed, K. (2013). A survey on inter-cell interference coordination techniques in OFDMA-based cellular networks. *IEEE Communications Surveys & Tutorials*, 15(4), 1642–1670.
3. Saquib, N., Hossain, E., & Kim, D. I. (2013). Fractional frequency reuse for interference management in LTE-advanced HetNets. *IEEE Wireless Communications*, 20(2), 113–122.
4. Mahmud, A., Lin, Z., & Hamdi, K. A. (2014). On the energy efficiency of fractional frequency reuse techniques. In *IEEE wireless communications and networking conference* (pp. 2348–2353).
5. Hamdi, K. A., & Mahmud, A. (2014). A unified framework for the analysis of fractional frequency reuse techniques. *IEEE Transactions on Communications*, 62(10), 3692–3705.
6. Novlan, T., Andrews, J. G., Sohn, I., Ganti, R. K., & Ghosh, A. (2010). Comparison of fractional frequency reuse approaches in the OFDMA cellular downlink. In *IEEE global telecommunications conference* (pp. 1–5).
7. Xu, Z., Li, G. Y., Yang, C., & Zhu, X. (2012). Throughput and optimal threshold for FFR schemes in OFDMA cellular networks. *IEEE Transactions on Wireless Communications*, 11(8), 2776–2785.
8. Tabassum, H., Dawy, Z., Alouini, M.-S., & Yilmaz, F. (2014). A generic interference model for uplink OFDMA networks with fractional frequency reuse. *IEEE Transactions on Vehicular Technology*, 63(3), 1491–1497.

9. Novlan, T. D., Ganti, R. K., Ghosh, A., & Andrews, J. G. (2011). Analytical evaluation of fractional frequency reuse for OFDMA cellular networks. *IEEE Transactions on Wireless Communications*, 10(12), 4294–4305.
10. Chang, H.-B., & Rubin, I. (2016). Optimal downlink and uplink fractional frequency reuse in cellular wireless networks. *IEEE Transactions on Vehicular Technology*, 65(4), 2295–2308.
11. Sagkriotis, S. E., & Panagopoulos, A. D. (2016). Optimal FFR policies: maximization of traffic capacity and minimization of base station's power consumption. *IEEE Communications Letters*, 5(1), 40–43.
12. Liu, L., Peng, T., Zhu, P., Qi, Z., & Wang, W. (2016). Analytical evaluation of throughput and coverage for FFR in OFDMA cellular network. In *IEEE vehicular technology conference* (pp. 1–5).
13. Lan, Y., Benjebbour, A., Li, A., & Harada, A. (2014). Efficient and dynamic fractional frequency reuse for downlink non-orthogonal multiple access. In *IEEE vehicular technology conference* (pp. 1–5).
14. Hamouda, S., Yeh, C., Kim, J., Wooram, S., & Kwon, D. S. (2009). Dynamic hard fractional frequency reuse for mobile WiMAX. In *IEEE international conference on pervasive computing and communications* (pp. 1–6).
15. Ali, S. H., & Leung, V. C. (2009). Dynamic frequency allocation in fractional frequency reused OFDMA networks. *IEEE Transactions on Wireless Communications*, 8(8), 4286–4295.
16. Assaad, M. (2008). Optimal fractional frequency reuse (FFR) in multicellular OFDMA system. In *IEEE vehicular technology conference* (pp. 1–5).
17. Bilios, D., Bouras, C., Kokkinos, V., Papazois, A., & Tseliou, G. (2012). Optimization of fractional frequency reuse in long term evolution networks, In *IEEE wireless communications and networking conference* (pp. 1853–1857).
18. Boddu, S. R., Mukhopadhyay, A., Philip, B. V. & Das, S. S. (2013). Bandwidth partitioning and SINR threshold design analysis of fractional frequency reuse, In *IEEE national conference on communications* (pp. 1–5).
19. Mei, H., Bigham, J., Jiang, P., & Bodanese, E. (2013). Distributed dynamic frequency allocation in fractional frequency reused relay based cellular networks. *IEEE Transactions on Communications*, 61(4), 1327–1336.
20. Zhuang, H., Shmelkin, D., Luo, Z., Pikhletsky, M., & Khafizov, F. (2013). Dynamic spectrum management for intercell interference coordination in LTE networks based on traffic patterns. *IEEE Transactions on Vehicular Technology*, 62(5), 1924–1934.
21. Dinc E., & Koca, M. (2013). On dynamic fractional frequency reuse for OFDMA cellular networks. In *IEEE international symposium on personal, indoor and mobile radio communications* (pp. 2388–2392).
22. Sohaib, S., So, D. K., & Ahmed, J. (2009). Power allocation for efficient cooperative communication. In *IEEE international symposium on personal, indoor and mobile radio communications* (pp. 647–651).
23. Yu, Y., Dutkiewicz, E., Huang, X., & Mueck, M. (2013). Downlink resource allocation for next generation wireless networks with inter-cell interference. *IEEE Transactions on Wireless Communications*, 12(4), 1783–1793.
24. Sohaib, S., & So, D. K. (2013). Asynchronous cooperative relaying for vehicle-to-vehicle communications. *IEEE Transactions on Communications*, 61(5), 1732–1738.
25. Ashraf, M., & Sohaib, S. (2014). Energy-efficient delay tolerant space time codes for asynchronous cooperative communications. *Transactions on Emerging Telecommunications Technologies*, 25(12), 1231–1237.
26. Mohamed, A. S., Abd-Elnaby, M., & El-Dolil, S. (2016). Self-organised dynamic resource allocation scheme using enhanced fractional frequency reuse in LTE-advanced relay-based networks. *IET communications*.
27. Glenn Aliu, O., Mehta, M., Imran, M. A., Karandhikar, A., & Evans, B. (2014). A new cellular-automata-based fractional frequency reuse scheme. *IEEE Transactions on Vehicular Technology*, 64(4), 1535–1547.
28. Rahman, M., & Yanikomeroglu, H. (2010). Enhancing cell-edge performance: a downlink dynamic interference avoidance scheme with inter-cell coordination. *IEEE Transactions on Wireless Communications*, 9(4), 1414–1425.
29. Mahmud, A., Hamdi, K. A., & Ramli, N. (2014). Performance of fractional frequency reuse with CoMP at the cell-edge. In *IEEE region 10 symposium* (pp. 93–98).
30. Wang, L.-C., & Yeh, C.-J. (2011). 3-cell network MIMO architectures with sectorization and fractional frequency reuse. *IEEE Journal on Selected Areas in Communications*, 29(6), 1185–1199.
31. Ullah, R., Faisal, N., Safdar, H., Maqbool, W., Khalid, Z., & Khan, A. (2013). Voronoi cell geometry based dynamic fractional frequency reuse for OFDMA cellular networks. In *IEEE international conference on signal and image processing applications* (pp. 435–440).
32. Yassin, M., Dirani, Y., Ibrahim, M., Lahoud, S., Mezher, D., & Cousin, B. (2015). A novel dynamic inter-cell interference coordination technique for LTE networks. In *IEEE international symposium on personal, indoor and mobile radio communications*.
33. A Gebremariam, A., Bao, T., Siracusa, D., Rasheed, T., Granelli, F., & Goratti, L. (2016). Dynamic strict fractional frequency reuse for software-defined 5g networks. In *IEEE international conference on communications*.
34. Andrews, J. G., Baccelli, F., & Ganti, R. K. (2010). A new tractable model for cellular coverage. In *Annual Allerton conference on communication, control, and computing* (pp. 1204–1211).
35. Rappaport, T. S., et al. (1996). *Wireless communications: principles and practice*. New Jersey: Prentice Hall PTR.
36. Simon, M. K., & Alouini, M.-S. (2005). *Digital communication over fading channels*. Hoboken: Wiley.
37. Aldosari, M. M., & Hamdi, K. A. (2014). Trade-off between energy and area spectral efficiencies of cell zooming and BSs cooperation. In *IEEE international conference on intelligent and advanced systems* (pp. 1–6).
38. Alouini, M.-S., & Goldsmith, A. J. (1999). Area spectral efficiency of cellular mobile radio systems. *IEEE Transactions on Vehicular Technology*, 48(4), 1047–1066.
39. Cover, T. M., & Thomas, J. A. (2012). *Elements of information theory*. Hoboken: Wiley.
40. Hamdi, K. A. (2010). A useful lemma for capacity analysis of fading interference channels. *IEEE Transactions on Communications*, 58(2), 411–416.
41. Chandhar, P., & Das, S. S. (2014). Area spectral efficiency of co-channel deployed OFDMA femtocell networks. *IEEE Transactions on Wireless Communications*, 13(7), 3524–3538.
42. Mahmud, A., & Hamdi, K. (2012). Uplink analysis for FFR and SFR in composite fading. In *IEEE international symposium on personal, indoor and mobile radio communications* (pp. 1285–1289).



Maryum Hina received the BSc and MSc degrees in electrical engineering from University of Engineering and Technology, Taxila, Pakistan in 2013 and 2016 respectively. From 2013 to 2015, she worked at University of Engineering and Technology, Taxila as research assistant and lab engineer. In 2015, she joined Sui Northern Gas Pipelines Limited (SNGPL), Pakistan and is currently working there as transmission engineer. Her research interests include radio resource

management, heterogeneous networks and digital electronics.



Sarmad Sohaib received the BSc degree in electrical and electronics engineering from Ghulam Ishaq Khan Institute of Engr. Sciences & Tech. (GIKI), Pakistan in 2005 and the Ph.D. degree in electrical and electronics engineering from the University of Manchester, Manchester, United Kingdom, in 2010. From 2005 to 2006, he worked at Mobilink-Pakistan Mobile Co. Ltd., Pakistan, as a telecom engineer. In 2010, he joined Department of Electrical Engineering,

University of Engineering and Technology, Taxila, Pakistan as an assistant professor. His research interests include cooperative MIMO communication, cognitive radio networks, and green communications.